Mineralogical and geochemical features of the Allan Hills tephra, South Victoria Land: Implications for mid-Pleistocene volcanic activity in Antarctica

Anastassia y Borisova, Klaus Peter Jochum, Sophie Gouy

Mineralogical and geochemical features of the Allan Hills tephra, South Victoria Land: Implications for mid-Pleistocene volcanic activity in Antarctica

Anastassia Y. Borisova [1,2]*, Klaus Peter Jochum [3] and Sophie Gouy [1]

[1] Géosciences Environnement Toulouse, Université de Toulouse; UPS OMP- CNRS - IRD, 14 Avenue E. Belin, 31400 Toulouse, France; anastassia.borisova@get.omp.eu, sophie.gouy@get.omp.eu

[2] Geological Department, Lomonosov Moscow State University, Vorobievy Gory, 119899, Moscow, Russia

[3] Climate Geochemistry Department, Max Planck Institute for Chemistry, D-55020 Mainz, Germany; k.jochum@mpic.de

* Correspondence: anastassia.borisova@get.omp.eu; Tel.: +33(0)5 61 54 26 31 (A.Y.B.)

Abstract: More than 100 volcanoes have been discovered in Antarctica, however, the sources of many Antarctic tephras are not yet constrained. In this study, four tephra samples recovered from the environment of Site 27 on an area of blue ice at Allan Hills, South Victoria Land, provide information on magma and crustal sources for the tephra erupted in Antarctica. We report data on the chemistry of Antarctic tephra glasses and minerals analysed by electron microscopy, electron probe microanalysis and laser ablation inductively coupled plasma mass spectrometry. The tephra amphibole chemistry indicates magma residence at ~1 GPa and ~1100 °C. Abundant Ca-Al-Si-rich minerals imply that the magma ascended from a reservoir at 29.4 ± 2.7 km depth was affected by the assimilation of calc-silicate crust. The high Fe and Ti contents in the magmatic minerals and the trace element patterns of the glasses typical of a hydrothermally altered oceanic crust suggest that the Allan Hills tephra originated from a mantle plume-derived magma. The fragmented morphology of the glasses implies that the magmatic activity was associated with explosive eruptions during the mid-Pleistocene. The chemistry of the glasses and the presence of rhönite and Al-rich spinel minerals suggest that the magma might be genetically related to the currently active McMurdo volcanic group.

Keywords: volcanic tephra; Antarctica; Allan Hills; mantle plume; Pleistocene;

1. Introduction

Antarctica is a volcanically active region (Kyle et al., 1990; Wörner, 1999; Van Wyk de Vries, 2017; Iverson et al., 2017). A number of "dust" bands visible on the surface of blue ice at Allan Hills, South Victoria Land are reported to be volcanic ashes (tephra) (Nishio et al., 1985; Dunbar et al., 1995; Spaulding 2012; 2013; Iverson et al., 2014; 2017). Tephra

layers in blue ice result from explosive eruptions, thus providing excellent time-lines for the assessment of climate change, thermal anomalies and volcanic activity in polar regions (Keys et al., 1977; Ponomareva et al., 2013; Dunbar et al., 2017; Narcisi et al., 2012; 2016; 2017). However, the sources and ages of many Antarctic tephras are not yet constrained. This fact hampers the use of tephra for establishing correlations with paleo-climatic archives. This study aims to (i) identify the mineralogical and chemical composition of the dated tephra particles from the environment of Site 27 in the Allan Hills blue ice area (BIA), South Victoria Land, (ii) interpret this information in terms of the physical-chemical conditions of magmatic crystallization and (iii) obtain better constraints on the origin of tephra. Moreover, the results presented here may be used to improve our interpretation of paleo-environmental records (Keeling and Whorf, 2004) in Antarctica. In this study, we investigate four tephra samples recovered from the environment of Site 27, allowing us to elucidate the presence of multiple magma sources in the Southern Victoria Land.

2. Materials and Methods

Four samples (labelled BIT10, BIT12, SURF and CORE) were collected from englacial tephras at Site 27 in the Allan Hills BIA (Fig. 1, Table 1). Glaciological studies suggest steady-state conditions allowing the long-term continuity of the ice areas as well as that old ice is located at the surface (Spaulding et al., 2012; 2013). Each tephra sample is derived from a cubic meter of ice. The ice is first melted, followed by decantation of the water and storage of the complete (unfiltered) sample. The insoluble residue of the tephra is extracted from melted ice samples using 0.2-μm Nuclepore polycarbonate filters. The melt water volume for each of these samples is from ~150 mL to ~250 mL. Map coordinates for each sample are given in Table 1. SURF was collected from the same ash layer as BIT10, while CORE was sampled 24.25 m up flow from SURF, extracted from an ice core at a depth of

~3.5 m. Stratigraphically, BIT10, SURF and CORE all represent the same tephra layer, which is dated at ~114.7 ka, according to a time scale developed for Site 27 or ice core S27 (Spaulding et al., 2012; 2013; Higgins et al., 2015), whereas the glass-rich BIT12 sample (Fig. 2) is dated by $^{40}Ar/^{39}Ar$ method at 202 ± 7 ka (Iverson, 2017).

The tephra samples were carefully embedded into epoxy resin, polished with SiC paper and diamond pastes and then investigated at the Géosciences Environnement Toulouse (GET) laboratory in France using a JEOL JSM-6360 LV scanning electron microscope, with energy dispersive spectroscopy (EDS) coupled with an automatic particle analyzer controlled by the "Esprit" program working in the "Feature" module. The backscattered electron (BSE) imaging was performed coupled with EDS mapping (Table 1, Supplementary Dataset) following the analytical protocol previously developed (Borisova et al., 2012; 2013) and described below. The solid particles (glasses and minerals) in each sample were initially distinguished based on their grey tones on the BSE images, being classified using the EDS technique (Table 1, Supplementary Dataset), and then analysed by electron probe microanalysis (EPMA) (Figs. 2, S1–S3). The most representative particles include glass, plagioclase, quartz, alkali feldspar, albite, spinels, iron silicate, clinopyroxene, orthopyroxene, kaersutite and Ca-Al-rich amphibole, ilmenite, rhönite and carbonates. These latter particles, together with other unclassified particles, are then used to interpret the tephra provenances. The minimum size of the analysed particles is 12 to 80 μm, with a maximum size ranging from 100 to 200 μm, depending on the sample (see Figs 2, S1-S3). The number of compositionally homogeneous particles analyzed by BSE-EDS method ranges from 190 to 270 per sample. Table 1 and the Supplementary Dataset summarize the mineral and glass contents in the four tephra samples obtained by back-scattered-electron-energy-dispersive X-ray spectroscopy (BSE-EDS) mapping.

Major- and minor-element compositions of glasses and minerals were determined on embedded samples using a CAMECA SX-50 instrument (GET, Toulouse, France), following the analytical protocol previously developed (Borisova et al., 2012; 2013). Additionally, the BIT12 glasses were analysed using a CAMECA SX-Five instrument (Centre Castaing, Toulouse, France). Tables 2, S1–S9 and the Supplementary Dataset present the complete dataset and analytical conditions applied during EPMA and femtosecond laser ablation inductively coupled plasma mass spectrometry (fs-LA-ICP-MS). For the spot analyses and mineral profiling, the electron beam was set at an accelerating voltage of 15 kV, with a probe current of 10–20 nA for minerals, 10 nA for glasses and a spot diameter on the sample of 4 μm (CAMECA SX-50) to defocused 10 μm (CAMECA SX-Five). Sodium was analysed first of all to assure minimal loss during EPMA; the applied analytical conditions allowed an optimal signal for the major and minor elements and a better internal precision. Such conditions are in accordance with recommendations given by Kuehn et al. (2011) for use in tephrochronology to ensure minimal sodium loss during EPMA. The following synthetic or natural reference materials were used: albite (Na), periclase (Mg), corundum (Al), sanidine (K), wollastonite (Si and Ca), pyrophanite (Ti), hematite (Fe), chromium oxide (Cr), and topaz (F). An acquisition time of 10 s was used per element on the peak (by CAMECA SX-50 and CAMECA SX-Five) in glasses and minerals and an acquisition time of 5 s was used per peak of Na (by CAMECA SX-Five) in the BIT12 glasses and 5 s per element on the background (by CAMECA SX-50 and CAMECA SX-Five). The analytical uncertainties (1–3 wt.% relative for major elements) are evaluated using MPI-DING reference glasses (T1-G, ATHO-G and StHs6/80-G, Table S3) as described by Jochum et al. (2006). The detection limits for major and minor elements in the main minerals, as well as glasses, are similar to those previously described by Borisova et al. (2012). The detection limit for F under the CAMECA SX-50 conditions is 700 ppm.

The major and trace element composition of the BIT12 glasses and minerals, as well as the glass-hosted inclusions of micrometric size, were measured and identified by fs-LA-ICP-MS at the Max Planck Institute for Chemistry, Mainz, Germany (Jochum et al., 2014) (see Table 2, Tables S1 and S2). Nine line scan analyses of 500 µm length each were performed on the BIT12 sample. Each of nine scan fs-LA-ICP-MS spectra has been thoughtfully analysed, and the spectra of the predominant "matrix" have been identified and separated from the "inclusion" spectra based on the characteristic peaks of Si and Na in those of "inclusions" (Fig. 2). The both analyzed "matrix" glasses and "inclusions" are essential components of the tephra analyzed by fs LA-ICP-MS (Fig. 2). The "matrix" composition was obtained based on 333 single measurements by fs LA-ICP-MS, whereas "inclusions" have been quantified based on the well-known method of inclusion analysis by laser ablation (e.g., Borisova et al., 2012; 2013). The analyzed "inclusions" are not always visible on the images obtained by electron microscopy (Fig. 2), since their identification and quantification is based solely on the fs LA-ICP-MS spectra. For the evaluation of the "matrix" and "inclusions" data, we have rejected the first 1 to 4 measurements per a scan line corresponding to a range of unstable conditions (unstable laser; relative higher proportion of (contaminated) surface material).

The LA-ICP-MS system was equipped with a femtosecond laser NWRFemto200 (Electro Scientific Industries, New Wave Research Division, Portland, OR, USA) (Jochum et al., 2014) and coupled with a Thermo Finnigan sector-field ICP-MS Element 2. Table S2 lists the main operating parameters, in addition to a detailed description of the Thermo Element 2 mass spectrometer at MPIC already given by Jochum et al. (2007). This system is fitted with a Ti-sapphire-based ultra-fast amplifier delivering laser pulses shorter than 130 fs. The amplifier produces a laser output wavelength of 200 nm via highly efficient harmonic generation of the fundamental wavelength. The laser beam is introduced into a high-

performance New Wave Large Format cell, which is a two-volume ablation cell capable of generating wash-out times <1 s and accommodating multiple samples and reference materials. We used NIST 610 as the calibration material and new reference values (Jochum et al., 2011). Spot size and repetition rate (used for the investigation of the tephra "matrix" and the reference glasses) were 40 µm and 50 Hz, respectively, at a fluence of 0.7 J cm^{-2}. We used line scan analysis, with a scan speed of 5 µm s^{-1}. The micro-size "inclusions" were investigated with a spot size of 25 µm at a fluence of 0.6 J cm^{-2}, with a scan speed of 1 µm s^{-1}.

The ICP-MS measurements were performed in low mass resolution mode ($M/\Delta M$ = 300), using a combination of magnetic and electrical scan modes. The analysis time for a 1-pass measurement is about 1.5 s, while the whole ablation time is 100 s for the "matrix" and 50 s for "inclusions" numbered 1 to 10. The following isotopes were used in the multi-element analyses: ^{7}Li, ^{11}B, ^{23}Na, ^{25}Mg, ^{27}Al, ^{29}Si, ^{43}Ca, ^{47}Ti, ^{51}V, ^{53}Cr, ^{55}Mn, ^{57}Fe, ^{59}Co, ^{62}Ni, ^{65}Cu, ^{66}Zn, ^{75}As, ^{85}Rb, ^{88}Sr, ^{89}Y, ^{90}Zr, ^{93}Nb, ^{133}Cs, ^{137}Ba, ^{139}La, ^{140}Ce, ^{141}Pr, ^{146}Nd, ^{147}Sm, ^{151}Eu, ^{157}Gd, ^{159}Tb, ^{163}Dy, ^{165}Ho, ^{167}Er, ^{169}Tm, ^{173}Yb, ^{175}Lu, ^{178}Hf, ^{181}Ta, ^{208}Pb, ^{232}Th, and ^{238}U. Offline data reduction was performed by the same mode by calculating the gas blank corrected ion intensities of the trace element isotopes of interest, relative to ^{43}Ca. Routine calculations programmed in Excel rejected obvious outliers by Jochum et al. (2007). In addition, the major element concentrations (including CaO wt.%) were adjusted (independently from trace elements) to a total oxide content of 97 wt.%, which is minimal content of the total oxide sum obtained by EPMA (Table S3, the Supplementary Dataset). The reproducibility (% RSD, relative standard deviation) of the fs-LA-ICP-MS analyses is 1–3% as demonstrated by the analyses of the most homogeneous glasses, such as, basaltic glass KL2-G (MPI-DING series) (Borisova et al., 2010; Jochum et al., 2006). For example, the concentration data for KL2-G agree with the reference values within 1–5% (Jochum et

al., 2014). Because of sample heterogeneities, the reproducibility of the "matrix" measurements of BIT12 tephra is lower (about 10–25%). The uncertainty of the data of the small (μm-size) "inclusions" is strongly dependent on the concentration and generally varies between 10% and 30%. The proposed contents of K_2O in the BIT12 tephra glasses given in Figure 3 are calculated according to the measured Na_2O contents and an average Na_2O/K_2O ratio characteristic of that measured in the BIT12 glasses by EPMA (see Table S3, Supplementary Dataset).

3. Results

The common feature of the investigated tephra samples is the presence of magmatic Ca amphiboles, titanomagnetites (up to 20 rel.%, Table 1), Ti-augites (up to 19 rel.%), plagioclases (up to 18 rel.%), and mildly peralkaline to alkaline glasses with quartz-normative compositions (up to 84 rel.%, see Fig. 2, Table S3, Supplementary Dataset).

BIT10 is a fine grained tephra (≤100 μm) with fragments and agglomerations of the volcanic particles composed of ferrokaersutite, kaersutite, ferro-edenite and plagioclase, as well as Ti-augite, apatite, anorthoclase, olivine, ilmenite, rhönite grains, and glasses of trachyandesitic, trachytic to phonolitic composition (Figs. 3, S1). The amphiboles are identified according to the classification of Leake et al. (1997). Table 1 and Tables S4–S9 show that the BIT10 sample contains magmatic Ca amphibole (Mg# 37–47, TiO_2 = 3.8–5.8 wt.%), Ti-augite (TiO_2 = 4.7–5.7 wt.%), olivine (Fo_{77-80}, CaO = 0.4–1.0 wt.%), plagioclase (An_{40-66}, FeO = 1.2 wt.%), titanomagnetite (Usp_{89}), ilmenite (Ilm_{92-94}) and F-apatite. Two Ca-Mg-Fe carbonate and two quartz particles are detected by the BSE-EDS method (Table 1, Supplementary Dataset). Moreover, abundant metamorphic Ca-Al-rich tschermakite amphiboles are identified in this sample. Three ilmenite particles (P216, P217 and P218) were detected and analysed by BSE-EDS mapping of the sample, being used here to estimate

191 the magmatic temperature and oxygen fugacity (f_{O2}) based on the Fe-Ti oxide
192 geothermobarometer (Ghiorso and Evans, 2008) (Table S8). Pairs of ilmenite–
193 titanomagnetite reflect the magmatic mineral equilibrium at a temperature of 1105 ± 15 °C
194 with redox conditions (expressed in logarithmic units, $\log(f_{O2})$, relative to the redox buffer of
195 nickel-nickel oxide, NNO) varying from NNO-1.3 to NNO-0.8 (Table S8).

196 BIT12 is a fragmented glass-rich tephra sample composed of 50 – 200 μm-sized glass
197 fragments of trachytic composition with typical bubble-wall appearance and fluidal texture
198 (SiO_2 = 58 – 68 wt.%; $Na_2O + K_2O$ = 7.6 – 9.4 wt.%), plagioclase (An_{33-57}, FeO = 0.14 –
199 0.34 wt.%), titanomagnetite (Usp_{83-86}) analysed by EPMA (Fig. 3, Tables S3, S5, S8), as
200 well as SiO_2 grains and glass-hosted "inclusions" identified and analysed by fs-LA-ICP-MS
201 (Figs. 2, 4, Table 2). Additionally, we have found particles of anorthoclase, Ca-Fe-rich
202 pyroxene and rhönite (see Table S9, Supplementary Dataset). Compared to the "particles"
203 identified by BSE-EDS and analysed by EDS and EPMA method, the analyzed "inclusions"
204 are not always visible on the images obtained by electron microscopy (Fig. 2), since their
205 identification and quantification is based solely on the fs LA-ICP-MS spectra.

206 The glasses analysed by EPMA and fs-LA-ICP-MS, using several line scans on a
207 micrometric scale, are characterized by a nearly homogeneous trachytic "matrix"
208 composition (Table 2, Figs. 2, 4) with high concentrations of Cs, Rb, Pb, REE, Nb, Th, U,
209 As and Zr relative to primitive mantle composition (Lyubetskaya and Korenaga, 2007). The
210 "matrix" glass has a quartz-normative composition (Table S3). The primitive mantle-
211 normalized pattern of the average composition is similar to the patterns of the McMurdo
212 trachyte rocks (Kyle, 1981; Kyle et al., 1992; Kelly et al., 2008), marine sediments (Ben
213 Othman et al., 1989) and global subducting sediment (GLOSS) (Plank and Langmuir, 1998).
214 The BIT12 glasses also show an inhomogeneous distribution of large-ion lithophile elements
215 (LILE) (Li, B, As, Ba, Rb, Sr and LREE), which can be distinguished on the laser ablation

patterns as sub-micrometric “inclusions” in the host “matrix” glass. An inclusion of the SiO_2 mineral (number 4, Fig. 2, Table 2) has very low Na_2O and Al_2O_3 contents (Na_2O^{SiO2} and $Al_2O_3{}^{SiO2}$ contents are below detection limits by fs-LA-ICP-MS). An inclusion of Si-Al-rich glass with relatively low Na_2O and high Rb (~270 ppm), Ba (~9000 ppm), Sr (~550 ppm), and Eu (3.4 ppm) contents (number 6, Table 2), is also detected by fs-LA-ICP-MS. The glass and mineral “inclusions” numbered 1 to 3 and 7 to 10 have elevated SiO_2 (66–68 wt.%), Al_2O_3 (15–22 wt.%), Na_2O (6.5–8.0 wt.%) contents comparable to alkali feldspar (Na-rich plagioclase or anorthoclase). The most abundant “matrix” glasses of trachyte composition are characterized by a X_{nf}/X ratio of 0.74 ± 0.04 (the X_{nf}/X value necessary for the estimation of amphibole-melt partitioning is the sum of the molar fractions of network-forming cations (X_{nf}) normalized to the molar fraction of the total number of cations (X) in the melt) according to Tiepolo et al. (2007). A single Ca-rich carbonate particle in this sample was also detected using BSE-EDS (Table 1, Supplementary Dataset).

SURF is a tephra sample with fragmented volcanic particles 50–200 μm in size. Table 1, Tables S4–S6, S8 and S9 report the mineralogy in the analysed zone of this sample, which contains plagioclase (An_{37-57}, FeO = 0.25–0.85 wt.%), magmatic Ca amphibole (Mg# 40–62, TiO_2 = 3.2–5.3 wt.%), titanomagnetite (Usp_{54-82}), rhönite, olivine (Fo_{68-85}, CaO = 0.3–1.0 wt.%), Ti-augites (TiO_2 = 2.7–3.8 wt.%), glasses of trachyandesite, trachyte to phonolite composition (Figs. 3, S3) and dolomite (SURF-20). Moreover, abundant metamorphic Ca-Al-rich tschermakite amphiboles are identified (see Supplementary Dataset). Four Ca-Mg-Fe carbonate particles are also detected using the BSE-EDS method (Table 1, Supplementary Dataset).

CORE is a finely grained tephra sample with particles of volcanic material finer than 50 μm. Table 1 and Tables S4–S8 show that the sample contains plagioclase (An_{33-68}, FeO = 0.6–1.0 wt.%), Ti-augite (TiO_2 = 2.3–5.5 wt.%), magmatic Ca amphibole (Mg# 38–76, TiO_2

= 3.9–5.6 wt.%), olivine (Fo_{84-87}, CaO = 0.2–0.4 wt.%), titanomagnetite (Usp_{49-70}), ilmenite ($Ilm_{0.91–1.0}$), glasses of trachyandesite to trachyte compositions (Figs. 3, S2), and rhönite particles. One Ca-Mg-Fe carbonate particle is detected using the BSE-EDS method (Table 1, Supplementary Dataset). Moreover, abundant metamorphic Ca-Al-rich tschermakite amphibole and four particles of Al-rich oxide of spinel group are identified (see Table S8 and Supplementary Dataset). The composition of the magmatic ilmenite particle (P171) detected and analysed by BSE-EDS method, coupled with that of titanomagnetite, yields a temperature of 1092 ± 100 °C and redox conditions slightly below the NNO buffer (from NNO-0.58 to NNO-0.19, Table S8).

Thus, in addition to typically magmatic minerals (ferrokaersutite, kaersutite, ferro-edenite, and plagioclase, along with Ti-augite, apatite, anorthoclase, olivine, ilmenite), and rhönite – a mineral belonging to the aenigmatite group (Kyle and Price, 1975) – as well as quartz-normative glasses of mildly peralkaline to alkaline composition (Table 2), all tephra samples contain metamorphic phases, such as carbonates, quartz, metamorphic Ca-Al-rich amphiboles and Al-rich spinels.

4. Discussion

4.1. Derivation of Allan Hills tephra from a mantle plume

A magmatic system that evolves as an open system (e.g., through assimilation-fractional crystallization, magma mixing) may nevertheless provide evidence of local equilibrium. For example, the mineral and glasses found in volcanic ashes formed due to crustal assimilation and magma mixing frequently coexist in local equilibrium at the μm scale (e.g., Borisova et al., 2012; 2013). In the investigated system, we applied partition coefficients between

magmatic minerals and mafic melts, principally those of alkaline affinity, to determine whether the mineral phases could be in equilibrium with the co-existing glasses.

In contrast to mid-ocean ridge magmas, mantle plume-derived or intraplate magmas typically represent high-temperature melts that are regularly enriched in Fe and Ti (e.g., Hawaii and Iceland) (Giehl et al., 2013). The investigated samples contain abundant differentiated glasses and associated Fe-Ti-rich minerals (e.g., Ti-augite, titanomagnetite, ilmenite and rhönite). The average TiO_2 content of 0.32 ± 0.23 wt.% in the BIT12 glasses (Table 2 and Table S3) corresponds to the value obtained by assuming a theoretical $D^{TiO2}_{Amph/melt}$ partition coefficient of 6 ± 2 according to the X_{nf}/X ratio described by Tiepolo et al. (2007). This Ti partitioning between amphibole and melt means that the BIT12 tephra glasses are close to equilibrium with the magmatic amphiboles in BIT10, SURF and CORE, with an average TiO_2^{Amph} content of 4.9 ± 0.6 wt.% (Table S4). The predominant "matrix" glass is also enriched in iron (average FeO^{glass} 5.2 ± 0.6 wt.%, Table 2 and Table S3), similar to the alkaline melts produced under water-saturated magmatic conditions (Giehl et al., 2013). According to experimental Fe partitioning between plagioclase and melt, $D^{FeO}_{Plag/melt}$ = 0.14–0.22 for $An_{40–60}$ (Bindeman et al., 1998), the BIT12 trachytic glasses are in equilibrium with the plagioclases $An_{55 \pm 12}$, with average FeO^{Plag} content of 0.84 ± 0.25 wt.% (BIT10, SURF, CORE, Table S5). A common volcanic origin is implied by the mid-Pleistocene age of the Allan Hills tephra samples (BIT12 is estimated to have been formed ~202 ka ago (Iverson, 2017), while samples BIT10, SURF, and CORE represent a tephra layer dated at ~115 ka) and the similar major element compositions of the mineral and glass particles in all tephra samples. The typical chemical features of the Allan Hills tephra glasses, mostly of trachytic to phonolitic composition, suggest that they originated from a common magma generated by mantle plume activity. The fragmented morphology and micrometric size of the analysed particles and glass fragments, as well as the typical bubble-wall

289 appearance and fluidal texture of the glasses (BIT12, Fig. 2), suggest a Plinian- or Subplinian-
290 type explosive eruption (e.g., Ponomareva et al., 2013; Borisova et al., 2012; 2013).

291 The occurrence of olivine Fo_{68-87} micro-crystals in samples BIT10, CORE and SURF,
292 which are likely from the same eruption, implies their common magmatic source. According
293 to experimental data on equilibrium Ca partitioning between olivine and aluminosilicate melt
294 ($D^{CaO}_{Ol/melt}$ = 0.14–0.28 at $Fo_{68–87}$) (Libourel, 1999), the Allan Hills olivines with CaO^{Ol} =
295 0.3–1.0 wt.% (Table S6) were crystallized from silicate melt with CaO^{melt} ranging from 1.1
296 to 5.2 wt.%. The fact that the BIT12 glasses have comparable CaO^{glass} of 1.0 ± 0.6 wt.%
297 (Tables 2, S3) indicates that the Allan Hills olivines (BIT10, CORE and SURF) are mostly
298 represented by magmatic crystals close to equilibrium with the analysed BIT12 trachytic
299 glasses. By contrast, the most CaO-rich (~ 1.0 wt.% CaO) olivine may have also crystallized
300 from Ca-rich melt formed due to the assimilation of calc-silicate crust (Deegan et al., 2010;
301 Borisova et al., 2013).

302 Furthermore, the BIT12 Allan Hills trachytic glasses are also strongly enriched in trace
303 elements such as Cs, Rb, Ba, Pb, B, La, Ce, Nb, Th, U, As and Zr compared to the primitive
304 mantle composition (Fig. 4). A hydrothermally altered oceanic lithosphere, which is similar
305 in composition to oceanic sediments, is enriched in volatiles (H_2O, B, As), LILE (such as Rb,
306 Ba, Cs, Pb, LREE), and high field strength elements (HFSEs; such as Al, Zr, Nb, Th, and U)
307 relative to heavy rare earth elements (HREE). High concentrations of volatiles (B, As), LILE,
308 and HFSE elements relative to HREE in the BIT12 glasses (e.g., "matrix" Table 2 and Table
309 S3) are signatures of either highly altered silicate rocks or pelagic sediments, such as GLOSS.
310 Similar to the Icelandic hot spot (Borisova et al., 2012), an altered oceanic lithosphere is an
311 appropriate candidate for a mantle plume source for the Allan Hills magma. This similarity
312 suggests that the Allan Hills magma draws its origin from a mantle plume derived from a
313 hydrothermally altered oceanic lithosphere. Indeed, the West Antarctic Rift System may be

314 related to a hot spot activity (Behrendt, 1999); the magmatic activity of Mount Erebus, Ross
315 Island, is related to a mantle plume known as the Erebus plume (Kyle et al., 1992). The Allan
316 Hills glass compositions are different from the Cenozoic rift magmas, which are
317 characterized by negative Pb anomalies in the primitive mantle-normalized patterns (Rocchi
318 et al., 2003). Therefore, the Allan Hills tephra glasses are chemically distinct from magmatic
319 products related to intraplate strike-slip tectonic activity. The alkalinity of the Allan Hills
320 glasses is similar to that of the McMurdo volcanic rocks and glasses (Fig. 3). Moreover, the
321 Allan Hills "matrix" trachytic glass displays mantle-normalized trace element patterns which
322 are similar to those of the McMurdo trachytes (Fig. 4); in addition, the Allan Hills tephra
323 contain a rare mineral called rhönite (Tables 1, S9, Supplementary Dataset). Similarly, the
324 Erebus and Melbourne volcanic products in the currently active McMurdo volcanic group
325 include rhönite-bearing- and Al-rich spinel-bearing trachytic lavas as well as pyroclastic fall
326 deposits related to explosive volcanism, (e.g., Kyle and Prie, 1975; Kyle, 1981; 1990; Iverson
327 et al., 2014; Kelly et al., 2008). These data strongly support a hypothesis that the studied
328 Allan Hills tephra may be genetically related to the currently active McMurdo volcanic
329 group. Thus, the Allan Hills tephra represent mid-Pleistocene ashes produced due to
330 intraplate magmatism, likely derived from mantle plume activity (Kyle et al., 1992), and
331 likely associated with the magmatic activity of the McMurdo volcanic group, in particular,
332 Erebus volcanic province.
333

334 *4.2. Physical-chemical conditions of magma crystallization*

335 In the Allan Hills tephra, the abundant mildly peralkaline to peralkaline glasses, together
336 with the presence of Ca amphiboles in the volcanic tephra, and the fragmented morphology
337 of the tephra particles (Figs. 2, S1–S3), imply an explosive eruption of the volcanic material
338 due to saturation of the magma with an aqueous fluid, (Martel et al., 1998). Application of

339 the amphibole geobarometer equation (Schmidt, 1992) to the Allan Hills amphiboles (Table
340 S4) yields an average pressure of 0.98 ± 0.09 GPa for magma residence in a deep reservoir,
341 likely in the presence of an H_2O-CO_2 fluid. Similarly, application of the amphibole
342 geobarometer of Ridolfi et al. (2010) implies a pressure of 1.1 ± 0.1 GPa. These high-pressure
343 conditions suggest that the magma may have resided in a chamber under mantle lithospheric
344 conditions (29.3 ± 2.7 km depth, Fig. 5), below the continental crust (Behrendt, 1999; Cooke
345 and Foden, 2016), rather than below a thick oceanic crust (e.g., Central Kerguelen Plateau)
346 (Borisova et al., 2014; 2017).

347 The high Ti contents in the BIT10, CORE, and SURF amphiboles ($Ti^C \geq 0.5$ apfu, atoms
348 per formula unit, Table S4) and Ti-augites (X^{cpx}_{CaTi} up to 0.20, Table S7) reflect an
349 enrichment in the Ca-Ti-Tschermak's molecule ($CaTiAl_2O_6$). This signature suggests a high
350 temperature during the magmatic crystallization. Given that TiO_2 contents in the amphibole
351 vary from 3.2 to 6.8 wt.%, the graphical method of Ernst and Liu (1998) implies magmatic
352 temperatures above 900 °C at a pressure of ~1 GPa. Calculations according to Equation (4)
353 from Féménias et al. (2006) and geothermometer of Ridolfi et al. (2010) suggest
354 crystallization temperatures of 1135 ± 80 °C and 1057 ± 50 °C, respectively (Table S4). The
355 clinopyroxene-only geothermometer indicates 1196 ± 90 °C at 0.9 GPa (Putirka, 2008)
356 (Table S7). These pressure-temperature conditions suggest deeper and hotter magmatic
357 reservoir(s) compared to the shallow magmatic system feeding the Erebus lava lake over the
358 last 20 kyr (Moussalam et al., 2013).

359 Moreover, the composition of rare ilmenite–titanomagnetite pairs from samples CORE
360 and BIT10 (Table S8) indicates reducing conditions below the NNO buffer (NNO-1.0 to
361 NNO-0.19, Table S8). These reducing conditions are also corroborated by the presence of
362 rhönite containing Ti^{3+} (Kyle and Price, 1975). These redox conditions are comparable to
363 those (between QFM and QFM-1.0) established by Moussallam et al. (2017) for the shallow

magmatic system feeding the Erebus lava lake over the last 20 kyr. The presence of abundant Ca-Al-rich tschermakite (Table 1, Supplementary Dataset) in the tephra suggests high temperature-pressure conditions of magma residence or transport in deep crustal rocks (e.g., Cooke and Foden, 2016).

4.3. Evidence for mineral dissolution and calc-silicate crust assimilation

Calc-silicate crust xenoliths observed in different volcanic products are systematically enriched in Ca-Al-rich minerals (e.g., amphibole, anorthite), carbonates, Ca-rich glasses and SiO_2-rich phases such as metamorphic quartz (Deegan et al., 2010; Borisova et al., 2013; 2016). Several carbonates, SiO_2 particles and an inclusion of SiO_2 with low Na_2O contents are also detected in the BIT10 and BIT12 tephra samples (Tables 1 and 2). Low Na_2O and Al_2O_3 contents in the SiO_2 "inclusion" (number 4, Fig. 2, Table 2) are detected by fs-LA-ICP-MS in the host "matrix" glass. This implies that the mineral phase is a quartz micro-xenocryst rather than magmatic cristobalite (Borisova et al., 2013) crystallized from the associated melt with high Na_2O and Al_2O_3 contents (Table 2).

The occurrence of dolomite and mylonitized limestones is documented in the Ross orogenic structures (Kleinschmidt et al., 2002), and metamorphic calc-silicate rocks are present elsewhere in Antarctica (Yamakawa et al., 2001). The presence of dolomite, other carbonates and quartz particles, as well as the "matrix" glass-hosted inclusion of quartz (number 4, Table 2 and Table S9) formed as micro-xenocrysts strongly supports crustal assimilation by the magma. Indeed, available experimental data suggest a dolomite-quartz stability limit at 500 °C at low pressures (Müller et al., 2004). Moreover, the thermal stability of limestone is below 820–870 °C at 0.1 MPa pressure (Ar and Doğu, 2001). Given that the established temperature conditions of the peralkaline magma crystallization are ~1100 °C,

388 the crustal dolomite was also likely thermodynamically unstable with the magma at high
389 pressure. Therefore, the crustal quartz-carbonate association may have briefly survived in the
390 magma as crustal micro-xenoliths, (e.g., Borisova et al., 2013; 2016), and could have been
391 incorporated into the volcanic tephra due to very rapid ascent of the Allan Hills magma from
392 its reservoir during an explosive (Plinian- or Subplinian-type) eruption.

393 The calc-silicate assimilation process is supported by the elevated concentration of Sr^{glass}
394 in one glass (Sr ≈ 550 ppm content in glass "inclusion" number 6) and the calculated Sr^{melt}
395 content up to 620 ppm (based on the Sr content in plagioclase "inclusion" 5, Table 2) in the
396 host BIT12 "matrix" glass (Deegan et al., 2010; Borisova et al., 2013; 2016). Moreover, the
397 observed Al-rich spinels are either representative of carbonate-rich metamorphic rocks (e.g.,
398 galaxite) (Essene and Peacor, 1983) or crystallized in the melt due to incongruent dissolution
399 of calc-silicate minerals such as anorthite (Morgan et al., 2006). The high abundance of the
400 main Ca-rich minerals (plagioclase, augites with elevated molar fractions of Ca-Tschermak
401 X^{cpx}_{CaTs} up to 0.1, and Ca-Al-rich tschermakite amphiboles, accounting for up to 58 rel.%,
402 Tables 1, S7), as well as accessory dolomite and other carbonates, quartz and the Al-rich
403 spinel particles in the tephra samples (Tables S8 and S9; Supplementary Dataset), are
404 signatures of calc-silicate crust assimilation (e.g., Mollo et al., 2010; Deegan et al., 2010). In
405 addition, the observed dispersion in alkalinity of the glasses of trachyandesitic, trachytic and
406 phonolitic to tephri-phonolitic composition (Fig. 3) may be also directly related to the
407 carbonate-bearing material assimilation by magmas (Mollo et al., 2010).

408 The compositions of the BIT12 glass "inclusion" imply inhomogeneity of the melt with
409 respect to most major, volatile and LILE trace elements (Li, B, As, Ba, Rb, Sr, REE, Fig. 4)
410 on a sub-micron scale, suggesting magma mixing. For example, the "inclusions" numbered
411 1 to 3 and 7 to 10 analysed by fs-LA-ICP-MS have elevated SiO_2, Al_2O_3, and Na_2O contents,
412 and are variably enriched in REE, Sr, Rb and Ba (Table 2). These inclusions may be formed

as glasses or as minerals due to progressive dissolution/crystallization of alkali feldspars in the melt. Indeed, the presence of anorthoclase particles in the BIT12 sample is recorded in our work (see Supplementary Dataset) and by Iverson (2017).

Additionally, formation of Si-Al-rich glass of dacite/rhyolite composition with high Sr, Rb, Ba and Eu contents (glass "inclusion" number 6, Table 2) is likely due to the dissolution of quartz ± plagioclase, and also requires thermodynamic instability triggered, for example, by crustal assimilation. Indeed, similar rhyolite series TD 1387B-iii is recently recorded by Narcisi et al. (2016) in the Talos Dome ice core (Northern Victoria Land); and it is dated at ~116 ± 2 ka. Although such felsic glasses are regularly considered to be genetically related to an extra-Antarctic source (Narcisi et al., 2012; 2016), the presence of the described inclusions within the Allan Hills trachytic "matrix" glass requires an *in situ* origin due to mineral (quartz ± plagioclase) dissolution during magma differentiation in the lithosphere of Antarctica. The volcanic particles might be accumulated during a single volcanic eruption and represent a result of syn-eruptive processes of mineral dissolution e.g., (Borisova et al., 2012; 2013). Mineral dissolution and mixing of melts by chemical diffusion can be directly related to magmatic events, in particular magma recharge and crustal assimilation (e.g., Deegan et al., 2010; Borisova et al., 2013; 2016; 2017). In the case of the Allan Hills tephras, which are chemically similar to the McMurdo volcanic group rocks and associated glasses (Fig. 3), the hypothesis of calc-silicate crust assimilation is strengthened by the presence of crustal xenoliths and xenocrysts in the Erebus and Melbourne Volcanic Province trachytes and more highly differentiated volcanics. These latter are characterized by variably radiogenic Sr isotope composition (Wörner et al., 1989; Kyle, 1990; Kyle et al., 1992; Wörner, 1999), providing additional arguments for either magma mixing or crustal assimilation associated with fractional crystallization or a combination of both.

Thus, the 202 – 115 ka Allan Hills magma might be derived from a mantle plume, likely currently located beneath the McMurdo volcanic group, and then accumulated in a deep magmatic reservoir at 29.4 ± 2.7 km depth. The magma was affected by calc-silicate crust assimilation in the crustal reservoir(s) under pre-eruptive and/or syn-eruptive conditions. Alternatively, lower crust of McMurdo volcanic region composed of altered oceanic crust (which may partially include calc-silicate materials) might be partially melted by underlying hot plume to produce the trachytic melts. This hypothesis may better explain differentiated and hydrous compositions of the Allan Hills tephra, and incorporation of partially dissolved crustal materials into the magma. The magma was explosively erupted due to an excess of H_2O-CO_2 fluid phase in the pre-eruptive reservoir(s) (Fig. 5). The existence of such reservoir(s) may be interpreted based on the total oxide contents of the well-polished glasses measured by EPMA (Table S3, Supplementary Dataset), which indicate up to 3 wt.% volatiles (H_2O-CO_2) dissolved in the melts upon quenching. Such dissolved volatile contents imply the melt saturation with H_2O-CO_2 fluid at pressure below 0.7 GPa corresponding to crustal depths (<20 km depth) (Iacovino et al., 2013), assuming the fraction of X_{H2O}^{fluid} ranges from 0.1 to 0.2.

5. Implications and conclusions

This study provides evidence for the origin of the mid-Pleistocene Allan Hills tephra in Antarctica, which are considered to represent volcanic products due to the explosive activity of a mantle plume-derived magma. Our data indicate that the mantle plume responsible for the origin of the S27 tephra is currently located beneath the McMurdo volcanic group. The chemistry of the magmatic Ca amphiboles implies that the magma resided at a depth of 29.3 ± 2.7 km. The presence of abundant magmatic Ca-rich minerals (e.g., plagioclase and augite), metamorphic Ca-Al-rich amphiboles, Ca-Fe pyroxenes as well as dolomite and other

carbonate minerals, Al-rich spinel, quartz xenocrysts and felsic glass "inclusions", suggests that the magma assimilated Ca-Si-Al-rich calc-silicate crustal material. The formation of Si-Al-rich glass of dacite/rhyolite composition (glass "inclusion" number 6, similar to rhyolite series TD 1387B-iii recorded by Narcisi et al. (2016) in the Talos Dome ice core, Northern Victoria Land, and dated at ~116 ka) requires an *in situ* origin due to mineral (quartz ± plagioclase) dissolution during magma differentiation in the lithosphere of Antarctica. The obtained data suggest that an attention should be made to interpret correctly isotopic composition of the contaminated lavas and glasses in terms of mantle plume composition.

We assume that the elevated atmospheric CO_2 concentrations recorded in the Antarctica region during the mid-Pleistocene (Higgins et al., 2015) might be due to at least two processes: (1) mantle plume activity and magma degassing due to saturation with a H_2O-CO_2 fluid phase (Ernst and Liu, 1998; Kelly et al., 2008), and (2) contact metamorphic decarbonation reactions due to interactions of the magma with calc-silicate crust. Since volcanic activity is frequently related to an elevated CO_2 flux (e.g., Ernst and Liu, 1998; Toutain et al., 2009), the mantle plume activity may also be responsible for the high CO_2 anomalies recorded in Antarctica ice cores. Such coupling of the volcanic tephra hosted in Antarctic ice cores and the host ice core composition is a highly promising approach for developing robust models of the terrestrial climate. This represents a high priority objective for Antarctic Science according to the current scientific programs (e.g., Antarctic Roadmap Challenges) (Kennicutt et al., 2016).

Supplementary Materials: Figure S1: Back-scattered electron image and the BSE-EDS mapping of the BIT10 Allan Hills tephra sample from site S27, Figure S2: Back-scattered electron image and the BSE-EDS mapping of the CORE Allan Hills tephra sample from site S27, Figure S3: Back-scattered electron image and the BSE-EDS mapping of the SURF Allan

Hills tephra sample from site S27, Table S1: Operating parameters of the laser ablation system used for the fs-LA-ICP-MS analyses, Table S2: Typical operating parameters of the ICP mass spectrometer used for the fs-LA-ICP-MS analyses, Table S3: Composition of glasses in the BIT12 sample (EPMA and CIPW norms in wt.%) and the ATHO-G reference material, Table S4: Compositions of calcic amphiboles in the tephra samples (EPMA in wt.%), formula units, Table S5: Compositions of anorthoclases and plagioclases in the tephra samples (EPMA in wt.%) Table S6: Compositions of olivines in the tephra samples (EPMA in wt.%), Table S7: Compositions of Ti-augites in the tephra samples (EPMA in wt.%), formula units, Table S8: Compositions of titanomagnetites and Al-rich spinel in the tephra samples (EPMA in wt.%), Table S9: Compositions of apatite, dolomite, and rhönite in the tephra samples (EPMA in wt.%), Supplementary Dataset: BSE-EDS mapping and EPMA data for the BIT10, BIT12, SURF and CORE samples.

Author Contributions: A.Y.B. performed the electron probe microanalyses, carried out the data analysis and led the drafting of the manuscript. K.P.J. provided access to LA-ICP-MS and analytical data. S.G. and A.Y.B. performed the EDS/SEM analyses and mapping, and the data were treated thereafter by S.G and A.Y.B. All the authors contributed to the discussion and interpretation of the results and edited early versions of the manuscript.

Funding: Funding for this work was provided by INSU “Aleas” and “Cessur” (2014 – 2017) in France.

Acknowledgments: The authors thank Editor Takashi Yamanouchi and several anonymous reviewers for important suggestions on the initial versions of the manuscript. The authors are

grateful to Brigitte Stoll and Ulrike Weis for technical assistance with the fs-LA-ICP-MS technique and Christine Cavaré-Hester and Anne-Marie Cousin for drafting the figures. The authors thank Andrei Kurbatov, Nelia Dunbar, Nicole Elizabeth Spaulding and William C. McIntosh for providing the tephra samples. Prof. Nelia Dunbar (2MBA project) provided information on four tephra samples. The authors thank Jean-Luc Bouchez, Saskia Erdmann, Azam Soltanmohammadi, and Anne Nedelec for important suggestions on earlier versions of the manuscript. This paper incorporates data from the Masters study of Elena Zakervashevitch carried out during 2011–2012 at Toulouse University III, Toulouse, France. Dr M.S.N. Carpenter post-edited the English style and grammar.

Conflicts of Interest: The authors declare no conflict of interest.

References

Ar, I., Doğu, G. 2001. Calcination kinetics of high purity limestones. Chemical Engineering Journal 83, 131-137.

Behrendt, J.C. 1999. Crustal and lithospheric structure of the West Antarctic Rift System from geophysical investigations — a review. Global and Planetary Change 23, 25–44.

Ben Othman, D., White, W. M., Patchett, J. 1989. The geochemistry of marine-sediments, island-arc magma genesis, and crust mantle recycling, Earth Planet. Sci. Lett. 94, 1–21.

Bindeman, I.N., Davis, A.M., Drake, M.J. 1998. Ion microprobe study of plagioclase-basalt partition experiments at natural concentration level of trace elements. Geochim. Cosmochim. Acta 62, 1175-1193.

Borisova A.Y., Freydier R., Polvé M., Candaudap F. 2010. In situ multi-elemental analysis of ATHO-G rhyolitic glass by femtosecond LA-ICP-MS: Evidence for significant heterogeneity at mm-scale in respect to Zn, Mo, Cs and Pb. Geostand. Geoanal. Res. 34, 245 – 255.

Borisova, A.Y., Toutain, J.-P., Stefansson, A., Gouy, S., de Parseval, P. 2012. Processes controlling the 2010 Eyfjallajökull explosive eruption. J. Geophys. Res.: Solid Earth 117, B05202.

Borisova, A.Y., Martel, C., Gouy, S., Pratomo, I., Sumarti, S., Toutain, J-P., Bindeman, I.N., de Parseval, Ph., Metaxian, J-P., Surono 2013. Highly explosive 2010 Merapi eruption: Evidence for shallow-level crustal assimilation and hybrid fluid. J. Volcanol. Geotherm. Res. 261, 193-208.

Borisova, A.Y., Faure, F., Deloule, E., Grégoire, M., Béjina, F., de Parseval, Ph., Devidal, J.-L. 2014. Lead isotope signatures of Kerguelen plume-derived olivine-hosted melt inclusions: Constraints on the ocean island basalt petrogenesis. Lithos 198–199, 153–171.

Borisova, A.Y., Gurenko, A.A., Martel, C., Kouzmanov, K., Cathala, A., Bohrson, W.A., Pratomo, I. Sumarti, S. 2016. Oxygen isotope heterogeneity of arc magma recorded in plagioclase from the 2010 Merapi eruption (Central Java, Indonesia). Geochim. Cosmochim. Acta 190, 13-34.

Borisova, A.Y., Bohrson, W.A., Grégoire, M. 2017. Origin of primitive ocean island basalts by crustal gabbro assimilation and multiple recharge of plume-derived melts. Geochem., Geophys., Geosyst., doi: 10.1002/2017GC006986.

Cooke, B., Foden, J. 2016. An amphibole perspective into magmatic processes at Sangeang Api volcano, Indonesia. AESC 2016 – Australian Earth Sciences

559 Convention, Uncover Earth's Past to Discover Our Future, 26-30 June, Adelaide
560 Convention Centre, www.aesc2016.gsa.org.au, 92.
561 Deegan, F.M., Troll, V.R., Freda, C., Misiti, V., Chadwick, J.P., McLeod, C.L.,
562 Davidson, J.P. 2010. Magma-carbonate interaction processes and associated CO_2
563 release at Merapi volcano, Indonesia: Insights from experimental petrology. J. Petrol.
564 51, 1027-1051.
565 Dunbar, N.W., Kyle, P.R., McIntosh, W.C., Esser, R.P. 1995. Geochemical composition
566 and stratigraphy of tephra layers in Antarctic blue ice: Insight into glacial
567 tephrochronology. Antarctic Journal – Review 76-78.
568 Dunbar, N.W., Iverson, N.A., Van Eaton, A.R., Sigl, M., Alloway, B.V., Kurbatov, A.V.,
569 Mastin, L.G., McConnell, J.R., Wilson, C.J.N. 2017. New Zealand supereruption
570 provides time marker for the Last Glacial Maximum in Antarctica. Sci. Reports 7,
571 12238.
572 Ernst, W.G., Liu, J. 1998. Experimental phase-equilibrium study of Al- and Ti-contents
573 of calcic amphibole in MORB – A semiquantitative thermobarometer. Am. Mineral.
574 83, 952-969.
575 Essene, E.J., Peacor, D.R. 1983. Crystal chemistry and petrology of coexisting galaxite
576 and jacobsite and other spinel solutions and solvi. Am. Mineral. 68, 449-455.
577 Féménias, O., Mercier, J-C.C., Nkono, C., Diot, H., Berza, T., Tatu, M., Demaiffe, D.
578 2006. Calcic amphibole growth and composition in calc-alkaline magmas: Evidence
579 from the Motru Dike Swarm (Southern Carpathians, Romania). Am. Mineral. 91, 73-
580 81.
581 Giehl, C., Marks, M., Nowak, M. 2013. Phase relations and liquid lines of descent of an
582 iron-rich peralkaline phonolitic melt: an experimental study. Contrib. Mineral.
583 Petrol. 65, 283–304.

584 Ghiorso, M.S., Evans, B.W. 2008. Thermodynamics of rhombohedral oxide solid
585 solutions and a revision of the Fe-Ti two-oxide geothermometer and oxygen-
586 barometer. American Journal of Science, 308, 957-1039.
587 Higgins, J.A., Kurbatov, A.V., Spaulding, N.E., Brook, E., Introne, D.S., Chimiak, L.M.,
588 Yan, Y., Mayewski, P.A., Bender, M.L. 2015. Atmospheric composition 1 million
589 year ago from blue ice in the Allan Hills, Antarctica. PNAS, 112, 6887 – 6891.
590 Iacovino, K., Moore, G., Roggensack, K., Oppenheimer, C., Kyle, P. 2013. H_2O-CO_2
591 solubility in mfic alkaline magma: applications to volatile sources and degassing
592 behavior at Erebus volcano, Antarctica. Contrib. Mineral. Petrol. 166, 845-860.
593 Iverson, N.A., Kyle, P.R., Dunbar, N.W., Mcintosh, W.C., Pearce, N.J.G. 2014. Eruptive
594 history and magmatic stability of Erebus volcano, Antarctica: Insights from englacial
595 tephra. Geochem., Geophys., Geosyst., doi: 10.1002/2014GC005435.
596 Iverson, N.A., Lieb-Lappen, R., Dunbar, N.W., Obbard, R., Kim, E., Golden, E. 2017.
597 The first physical evidence of subglacial volcanism under the West Antarctic Ice
598 Sheet. Scientific Reports 7, 11457, doi:10.1038/s41598-017-11515-3.
599 Iverson, N.A. 2017. Cherecterization and correlation of englacial tephra from blue ice
600 areas and ice cores, Antarctica. PhD thesis. New Mexico Institute of Mining and
601 Technology, Department of Earth and Environmental Science Socorro, New Mexico
602 November, 2017. ProQuest Number: 1068275.
603 Jochum, K.P., Stoll, B., Herwig, K., Willbold, M., Hofmann, A.W., Amini, M., Aarburg,
604 S., Abouchami, W., Hellebrand, E., Mocek, B., Raczek, I., Stracke, A., Alard, O.,
605 Bouman, C., Becker, S., Dücking, M., Brätz, H., Klemd, R., de Bruin, D., Canil, D.,
606 Cornell, D., de Hoog, C.-J., Dalpé, C., Danyushevsky, L., Eisenhauer, A., Gao, Y.,
607 Snow, J.E., Groschopf, N., Günther, D., Latkoczy, C., Guillong, M., Hauri, E.H.,
608 Höfer, H.E., Lahaye, Y., Horz, K., Jacob, D.E., Kasemann, S.A., Kent, A.J.R.,

609 Ludwig, T., Zack, T., Mason, P.R.D., Meixner, A., Rosner, M., Misawa, K., Nash,
610 B.P., Pfänder, J., Premo, W.R., Sun, W.D., Tiepolo, M., Vannucci, R., Vennemann,
611 T., Wayne, D. and Woodhead, J.D. 2006. MPI-DING reference glasses for in situ
612 microanalysis: New reference values for element concentrations and isotope ratios.
613 Geochem., Geophys., Geosyst. 7／2, doi: 10.1029/2005GC001060.
614 Jochum K.P., Stoll B., Herwig K., Willbold M. 2007. Validation of LA-ICP-MS trace
615 element analysis of geological glasses using a new solid-state 193 nm Nd:YAG laser
616 and matrix-matched calibration. J. Anal. At. Spectrom. 22, 112-121.
617 Jochum, K.P., Weis, U., Stoll, B., Kuzmin, D., Yang, Q., Raczek, I., Jacob, D.E., Stracke,
618 A., Birbaum, K., Frick, D.A., Günther, D., Enzeiler, J. 2011. Determination of
619 reference values for NIST SRM 610-617 glasses following ISO guidelines.
620 Geostand. Geoanal. Res. 35, 397-429.
621 Jochum, K.P., Stoll, B., Weis, U., Jacob, D.E., Mertz-Kraus, R., Andreae, M.O. 2014.
622 Non-matrix-matched calibration for the multi-element analysis of geological and
623 environmental samples using 200 nm femtosecond LA-ICP-MS: A comparison with
624 nanosecond lasers, Geostand. Geoanal. Res. 38, 265-292.
625 Johannsen, A. A. 1931. Descriptive Petrography of the Igneous Rocks. Vol. 1. Chicago
626 University Press, Chicago. pp. 267.
627 Keeling, C. D., Whorf, T. P. 2004. Atmospheric CO_2 records from sites in the SIO air
628 sampling network, In: Trends: A compendium of data on global change, carbon
629 dioxide information analysis center, Oak Ridge National Laboratory, US Department
630 of Energy, Oak Ridge, USA, http://cdiac.esd.ornl.gov/trends/co2/sio-mlo.htm
631 Kelly, P.J., Kyle, P.R., Dunbar, N.W., Sims, K.W.W. 2008. Geochemistry and
632 mineralogy of the phonolite lava lake, Erebus volcano, Antarctica: 1972 – 2004 and
633 comparison with other lavas. J. Volcan. Geotherm. Res. 177, 589 – 605.

Kennicutt, M.C., Kim, Y.D., Rogan-Finnemore, M., Anandakrishnan, S., Chown, S.L., Colwell, S., Cowan, D., Escutia, C., Frenot, Y., Hall, J., Liggett, D., Mcdonald, A.J., Nixdorf, U., Seigert, M.J., Storey, J., Wåhlin, A., Weatherwax, A., Wilson, G.S., Wilson, T., Wooding, R., Ackley, S., Biebow, N., Blankenship, D., Bo, P.S., Baeseman, J., Cárdenas, C.A., Cassano, J., Danhong, C., Danobeitia, J., Francis, J., Guldahl, J., Hashida, G., Jiménez Corbalán, L., Klepikov, A., Lee, J., Leppe, M., Lijun, F., López-Martinez, J., Memolli, M., Motoyoshi, Y., Mousalle Bueno, R., Negrete, J., Ojeda Cárdenes, M.A., Proano Silva, M., Ramos-Garcia, S., Sala, H., Shin, H., Shijie, X., Shiraishi, K., Stockings, T., Trotter, S., Vaughan, D.G., Viera da Unha de Menezes, J., Vlasich, V., Weijia, Q., Winther, J.-G., Miller, H., Rintoul, S., Yang, H. 2016. Synthesis delivering 21st century Antarctic and Southern Ocean science. Antarctic Science 28, 407 – 423. doi: 10.1017/S0954102016000481.

Keys, J.R., Anderton, P.W., Kyle, P.R. 1977. Tephra and debris layers in the Skelton Neve and Kempe glacier, South Victoria Land, Antarctica. New Zealand J. Geol. Geophys. 20, 971 - 1002.

Kleinschmidt, G., Buggisch, W., Läufer, A.L., Helferich, S., Tessensohn, F. 2002. The "Ross orogenic" structures in the Shackleton Range and their meaning for Antarctica. In: Antarctica at close of millennium. (J.A. Gamble, D.N.B. Skinner, S. Henrys, eds.) Royal Society of New Zealand Bulletin 35, 75 – 83.

Kuehn, S.C., Froese, D.G., Shane, P.A.R. 2011. INTAV Intercomparison Participants The INTAV intercomparison of electron-beam microanalysis of glass by tephrochronology laboratories: Results and recommendations. Quat. Internat. 246, 19 – 47.

Kyle, P.R. 1981. Mineralogy and geochemistry of a basanite to phonolite sequence at Hut Point Peninsula, Antarctica, based on core from Dry Valley Drilling Project Drillholes 1, 2 and 3. J. Petrol. 22, 451 – 500.

Kyle, P.R. 1990. Erebus Volcanic Province. In: Volcanoes of the Antarctic Plate and Southern Oceans. (W.E. LeMasurier, J.W. Thomson, eds.), Antarctic Research Series, 48, American Geophysical Union, Washington, D.C., pp. 81-145.

Kyle, P.R., Price, R.C. 1975. Occurrences of rhönite in alkali lavas of the McMurdo Volcanic Group, Antarctica, and Dunedin Volcano, New Zealand. Am. Mineral. 60, 722 – 725.

Kyle, P.R., Moore, J.A., Thirlwall, M.F. 1992. Petrologic evolution of anorthoclase phonolite lavas at Mount Erebus, Ross Island, Antarctica. J. Petrol. 33, 849 – 875.

Leake, B.E., Woolley, A.R., Arps, C.E.S., Birch, W.D., Gilbert, M.C., Grice, J.D., Hawthorne, F.C., Kato, A., Kisch, H.J., Krivovichev, V.G., Linthout, K., Laird, J., Mandarino, J.A., Maresh, W.V., Nickel, E.H., Rock, N.M.S., Schumacher, J.C., Smith, D.C., Stephenson, N.C.N., Ungaretti, L., Whittaker, E.J.W., Youzhi, G. 1997. Nomenclature of amphiboles: report of the subcommittee on amphiboles of the International Mineralogical Association, Commission on new minerals and mineral names. Can. Mineral. 35, 219-246.

Libourel, G. 1999. Systematics of calcium partitioning between olivine and silicate melt: implications for melt structure and calcium content of magmatic olivines. Contrib. Mineral. Petrol. 136, 63-80.

Lyubetskaya, T., Korenaga, J. 2007. Chemical composition of Earth's primitive mantle and its variance: 1. Method and results, J. Geophys. Res. 112, B03211.

Martel, C., Pichavant, M., Bourdier, J.-L., Traineau, H., Holtz, F., Scaillet, B. 1998. Magma storage conditions and control of eruption regime in silicic volcanoes: Experimental evidence from Mt. Pelée: Earth Planet. Sci. Lett. 156, 89–99.

Mollo, S., Gaeta, M., Freda, C, Di Rocco, T. 2010. Carbonate assimilation in magmas: A reappraisal based on experimental petrology. Lithos 114, 503–514.

Morgan, Z., Liang, Y., Hess, P. 2006. An experimental study of anorthosite dissolution in lunar picritic magmas: Implications for crustal assimilation process. Geochim. Cosmochim. Acta 70, 3477 – 3491.

Moussallam, Y., Oppenheimer, C., Scaillet, B., Kyle, P.R. 2013. Experimental phase-equilibrium constraints on the phonolite magmatic system of Erebus volcano, Antarctica. J. Petrol. 54, 1285-1307.

Müller, T., Baumgartner, L.P., Foster, C.T. Jr., Vennemann T.W. 2004. Metastable prograde mineral reaction in contact aureoles. Geology. 32, 821-824.

Narcisi, B., Petit, J.R., Delmonte, B., Scarchilli, C., Stenni, B. 2012. A 16,000-yr tephra framework for the Antarctic ice sheet: a contribution from the Talos Dome core. Quat. Sci. Rev. 49, 52 – 63.

Narcisi, B., Petit, J.R., Langone, A., Stenni, B. 2016. A new Eemian record of Antactic tephra layers retrieved from Talos Dome ice core (Northern Victorial Land). Global and Planetary Change 137, 69-78.

Narcisi, B., Petit, J.R., Langone, A. 2017. Last glacial tephra layers in the Talos Dome ice core (peripheral East Antarctic Plateau), with implications for chronostratigraphic correlations and regional volcanic history. Quat. Sci. Rev. 165, 111 – 126.

Nishio, F., Katsushima, T., Ohmae, H. 1985. Volcanic ash layers in base ice areas near the Yamato Mountains, Dronning Maud Land and the Allan Hills, Victoria Land, Antarctica. Ann. Glaciol. 7, 34-41.

Plank, T., Langmuir, C. H. 1998. The chemical composition of subducting sediment and its consequences for the crust and mantle. Chem. Geol. 145, 325-394.

Ponomareva, V., Portnyagin, M., Derkachev, A., Juschus, O., Garbe-Schönberg, D., Nürnberg, D. 2013. Identification of a widespread Kamchatkan tephra: A middle Pleistocene tie-point between Arctic and Pacific paleoclimatic records. Geophys. Res. Lett. 40, 3538-3543.

Putirka, K.D. 2008. Thermometers and barometers for volcanic systems. Rev. Mineral. Geochem. 69, 61-120.

Ridolfi, F., Renzulli, A., Puerini, M. 2010. Stability and chemical equilibrium of amphibole in calc-alkaline magmas: an overview, new thermobarometric formulations and application to subduction-related volcanoes. Contrib. Mineral. Petrol. 160, 45-66.

Rocchi, S., Storti, F., Di Vincenzo, G., Rossetti, F. 2003. Intraplate strike-slip tectonics as an alternative to mantle plume activity for the Cenozoic rift magmatism in the Ross Sea region, Antarctica. Geological Society, London, Special Publications 210, 145-158.

Schmidt, M.W. 1992. Amphibole composition in tonalite as function of pressure: an experimental calibration of the Al-in-hornblende barometer. Contrib. Mineral. Petrol. 110, 304-310.

Spaulding, N.E., Spikes, V.B., Hamilton, G.S., Mayewski, P.A., Dunbar, N.W., Harvey, R.P., Schutt, J., Kurbatov, A.V. 2012. Ice motion and mass balance at the Allan Hills blue ice area, Antarctica, with implications for paleoclimate reconstructions. J. Glaciol. 58, 399–406.

Spaulding, N. E., Higgins, J.A., Kurbatov, A.V., Bender, M.L., Arcone, S.A., Campbell, S., Dunbar, N.W., Chimiak, L.M., Introne, D.S., Mayewski, P.A. 2013. Climate

archives from 90 to 250 Ka in horizontal and vertical ice cores from the Allan Hills Blue Ice Area, Antarctica. Quat. Res. 80, 562-574.

Tiepolo, M., Oberti, R., Zanetti, A., Vannucci, R., Foley, S.F. 2007. Trace-element partitioning between amphibole and silicate melt. Rev. Mineral. Geochem. 67, 417-452.

Toutain, J.P., Sortino, F., Baubron, J-C., Richon, P., Surono, Sumarti, S., Nonell, A. 2009. Structure and CO_2 budget of Merapi volcano during inter-eruptive periods. Bull. Volcanol. 71, 815–826.

Van Wyk de Vries, M., Bingham, R. G., Hein, A. S. 2017. A new volcanic province: an inventory of subglacial volcanoes in West Antarctica. In: (Siegert M. J., Jamieson S. S. R. & White D. A., eds.) Exploration of Subsurface Antarctica: Uncovering Past Changes and Modern Processes. Geological Society, London, Special Publications, 461, https://doi.org/10.1144/SP461.7.

Wörner, G. 1999. Lithospheric dynamics and mantle sources of alkaline magmatism of the Cenozoic West Antarctic Rift System. Global and Planetary Change 23, 61–77.

Wörner, G., Viereck, L., Hertogen, J., Niephaus, H. 1989. The Mt. Melbourne Volcanic Field (Victoria Land, Antarctica) II Geochemistry and magma genesis. Geol. Jb. E38, 395 – 433.

Yamakawa, J., Ando, Y., Osanai, Y., Kusachi, I. 2001. The crystal structure of scapolite in the Lutzow-Holm Bay region, East Antarctica. Polar Geosci. 14, 139-156.

FIGURE CAPTIONS:

Figure 1. Map of the Allan Hills Blue Ice Area (BIA) in South Victoria Land, Antarctica. The ash layers crossing transect A–B are shown. The ice core S27 was collected from the main icefield (marked as MIF) of the Allan Hills BIA during field seasons in 2010 and 2011. Maps are modified after Spaulding et al. (2012).

Figure 2. (A) Back-scattered electron image of the BIT12 Allan Hills tephra sample from site S27. (B) Result of BSE-EDS mapping for sample BIT12. The color coding identifies a given class of particles (see Figs. S1-S3), representing the glasses and minerals. The image represents volcanic glass (beige), alkali feldspar (yellow) and the plagioclase (violet) and not identified (grey). (C) The fs LA-ICP-MS spectra of quartz inclusion number 4. For the evaluation of the data, we have rejected the first 4 measurements corresponding to the range of unstable conditions (unstable laser; relative higher proportion of (contaminated) surface material). The identification and quantification of the "inclusions" and "matrix" are based solely on the fs-LA-ICP-MS spectra. The glasses and minerals analyzed by the scan lines are not always visible on the BSE images.

Figure 3. Total alkalis versus silica (TAS) diagram (Na_2O+K_2O versus SiO_2, wt.%) for the S27 Allan Hills tephra glass particles analysed using EPMA, fs-LA-ICP-MS and BSE-EDS. The composition of the predominant "matrix" analysed by fs-LA-ICP-MS is indicated. The BIT12 glasses analysed using EPMA and fs-LA-ICP-MS

774 are of trachytic composition. The glass compositions are compared to the bulk-rock
775 and matrix glass composition of the Erebus volcano lavas (labelled as McMurdo
776 volcanic rocks and glasses), from Kyle (1981; 1990); Kyle et al. (1992) and Kelly
777 et al. (2008). The plotted BSE-EDS data points can be found in the Supplementary
778 Dataset. CA = carbonate crust assimilation; FC = fractional crystallization; CSA =
779 calc-silicate assimilation via quartz-bearing rock dissolution.

780

781 **Figure 4.** Pattern of the trace element compositions normalized to primitive mantle
782 for S27 Allan Hills BIT12 glasses analyzed by femtosecond laser ablation-
783 inductively coupled plasma-mass spectrometry (fs-LA-ICP-MS). The "matrix" (red
784 diamonds) and "inclusions" (rose field) are normalized to composition from
785 (Lyubetskaya and Korenaga, 2007). The "matrix" and "inclusions" patterns are
786 compared to the patterns of the bulk-rock composition of the McMurdo volcanic
787 group trachyte lavas and pyroclastic rocks (labelled as McMurdo trachyte lavas)
788 (Kyle, 1981; 1990; Kyle et al., 1992; Kelly et al., 2008), marine sediments (Ben
789 Othman et al., 1989), and global subducted sediments (GLOSS) (Plank and
790 Langmuir, 1998). The order of elements on the plot corresponds to the increasing
791 ratio of charge to ionic radius (Borisova et al., 2012). The arrow indicates an increase
792 in the Sr concentration in the glass "inclusion" (number 6) compared to the average
793 Sr content in the "matrix" glass (Table 2).

794

795 **Figure 5.** Scheme of the proposed model for residence and transport of the Allan
796 Hills magma during mid-Pleistocene explosive eruptions. The magma was derived
797 from a mantle plume currently located beneath the McMurdo volcanic group. The

magma crystallized in a magma chamber located within a deep reservoir at a depth of 29.4 ± 2.7 km. The magma was then affected by calc-silicate crust assimilation and mixing, and explosively erupted likely due to an excess of CO_2-bearing fluids in the pre-eruptive reservoir(s) or during eruption.

805 **FIGURES:**

806

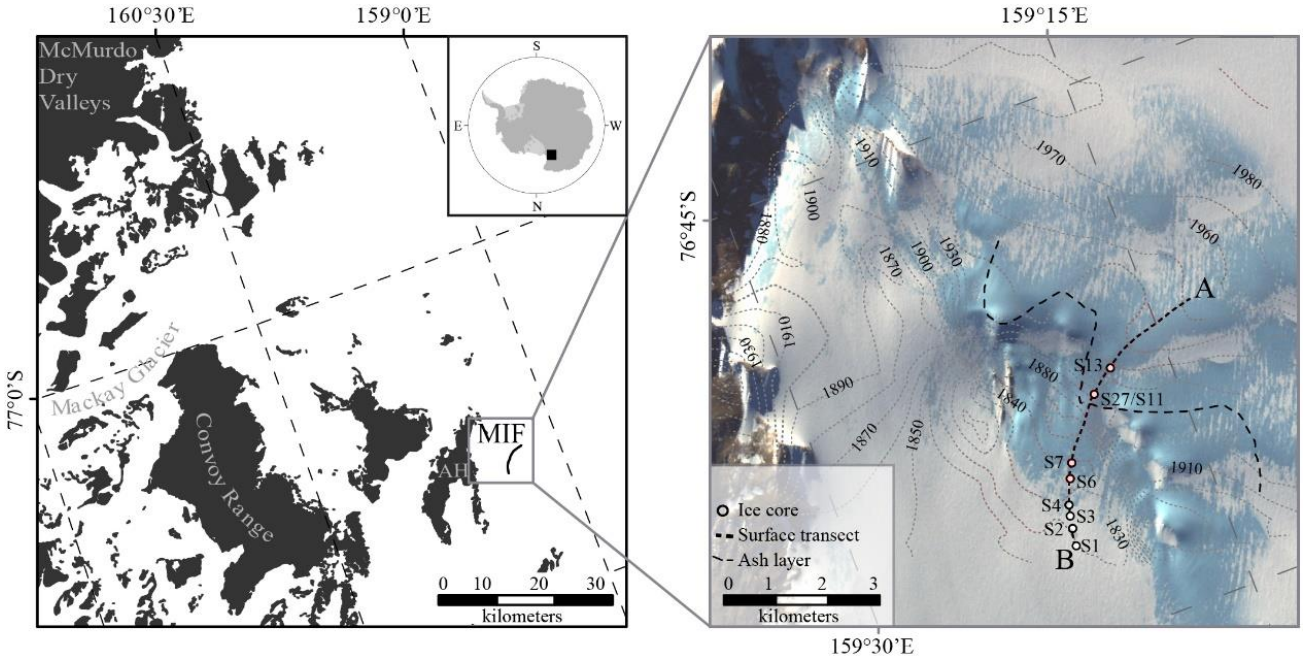

807

808 **Figure 1.**

809

810

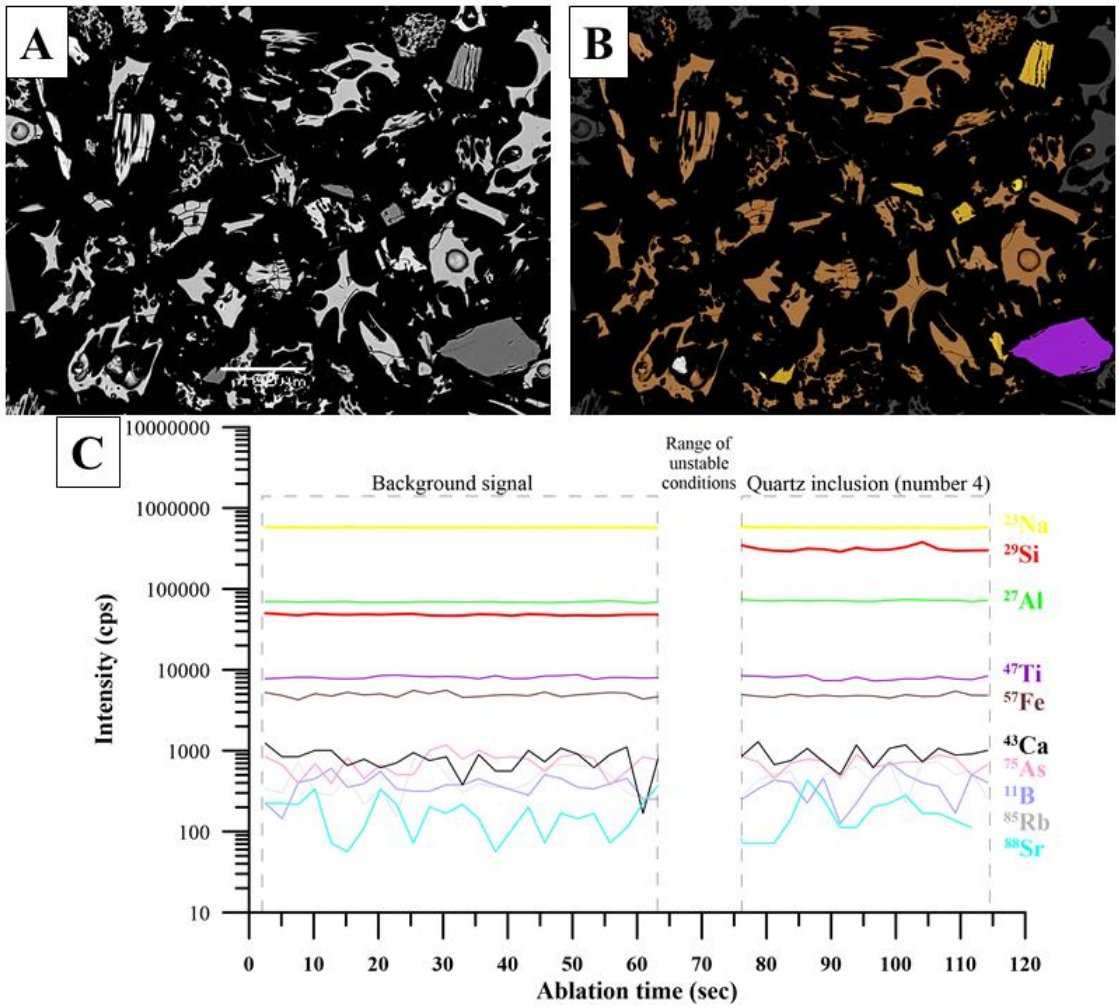
A
B
C
Background signal
Range of unstable conditions
Quartz inclusion (number 4)
Intensity (cps)
Ablation time (sec)
10000000
1000000
100000
10000
1000
100
10
0
10
20
30
40
50
60
70
80
90
100
110
120
23Na
29Si
27Al
47Ti
57Fe
43Ca
75As
11B
85Rb
88Sr

Figure 2.

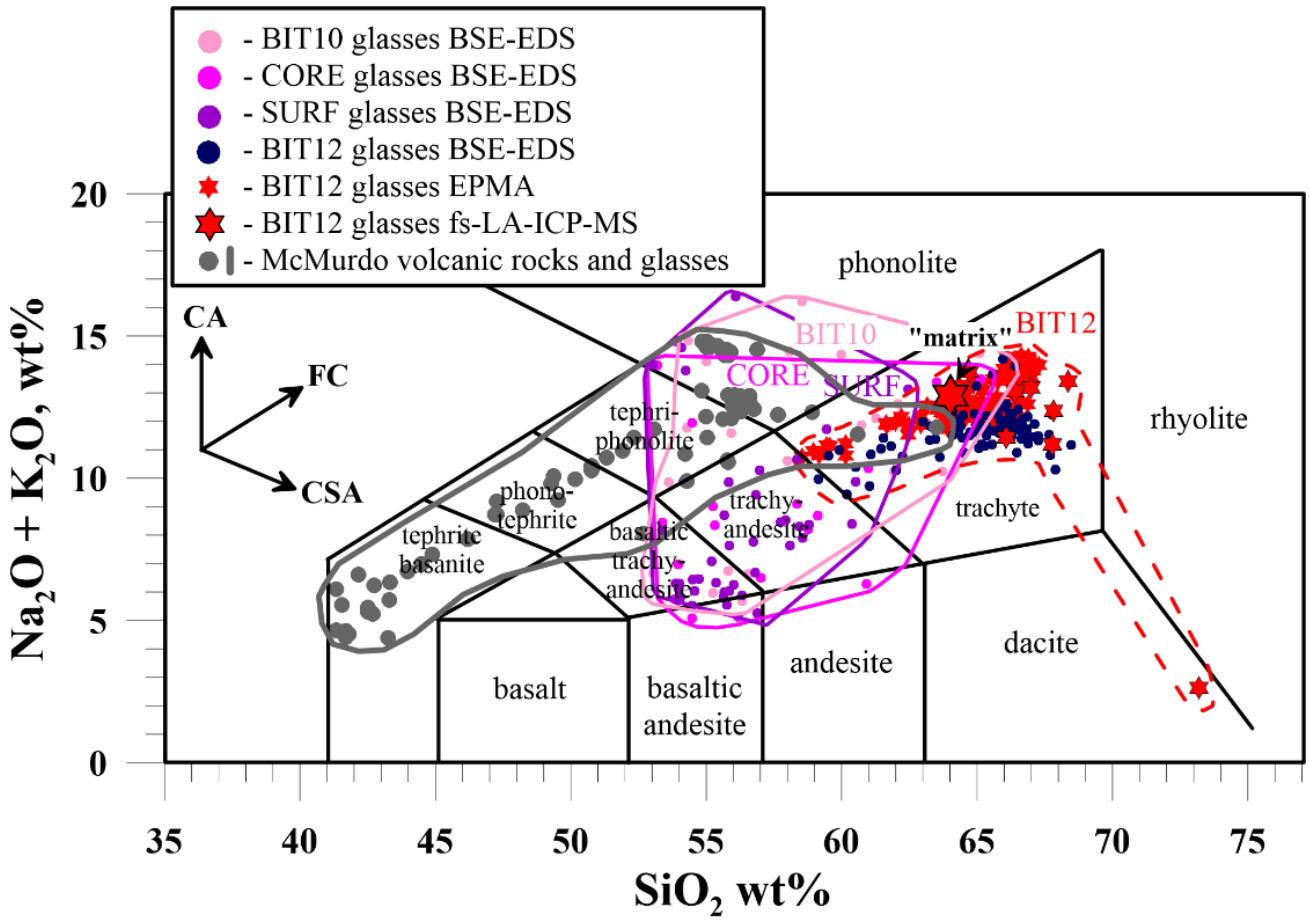
- BIT10 glasses BSE-EDS
- CORE glasses BSE-EDS
- SURF glasses BSE-EDS
- BIT12 glasses BSE-EDS
- BIT12 glasses EPMA
- BIT12 glasses fs-LA-ICP-MS
- McMurdo volcanic rocks and glasses
CA
FC
CSA
BIT10
CORE
SURF
"matrix"
BIT12
phonolite
rhyolite
tephri-phonolite
phono-tephrite
tephrite basanite
basaltic trachy-andesite
trachy-andesite
trachyte
basalt
basaltic andesite
andesite
dacite
$Na_2O + K_2O$, wt%
SiO_2 wt%
0
5
10
15
20
35
40
45
50
55
60
65
70
75

Figure 3.

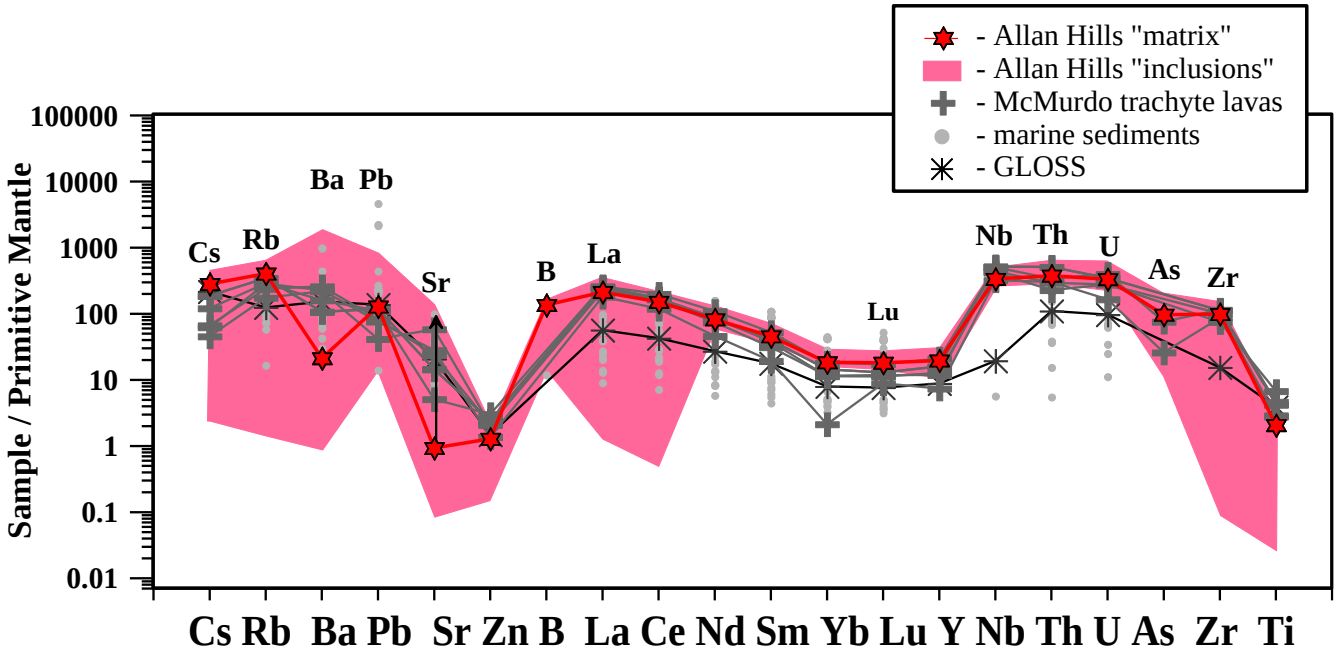

819

820 **Figure 4.**

821

822

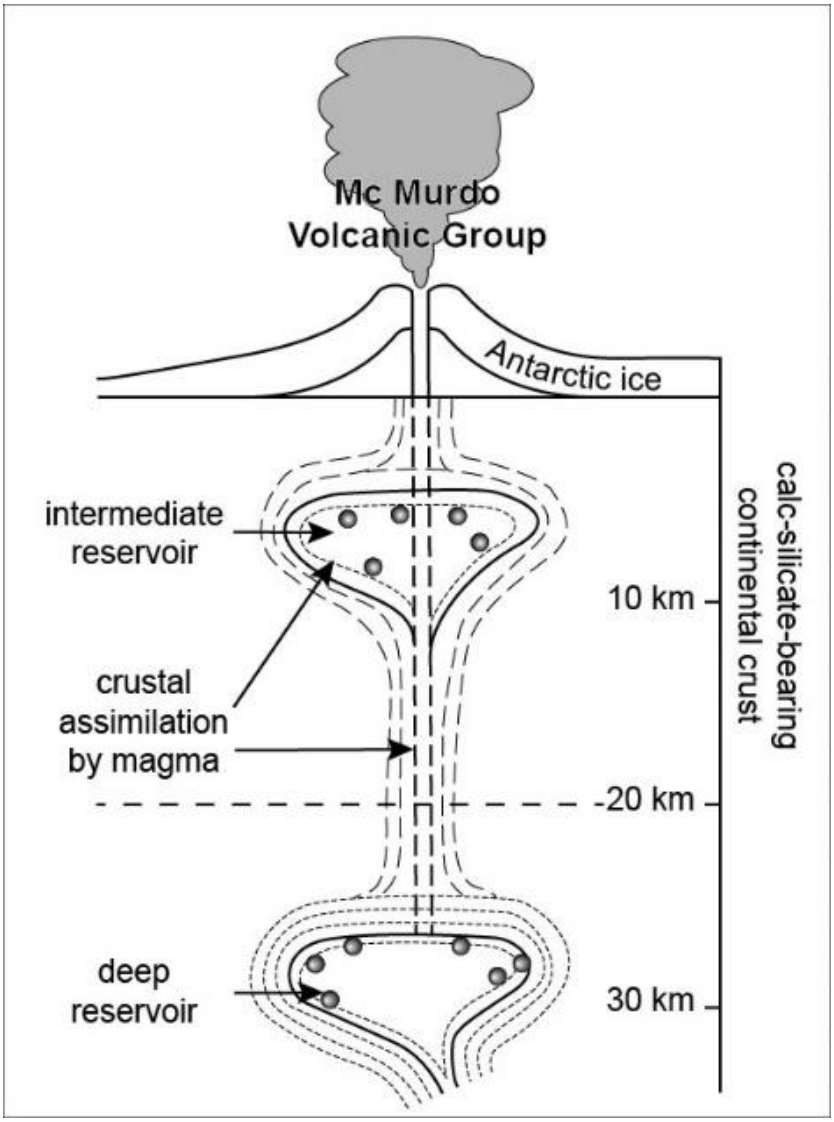

823 **Figure 5.**

824

Table 1. Coordinates and contents of minerals and glass in the Allan Hills BIA tephra samples (Antarctica).

	Samples							
Sample coordinates:	BIT10		BIT12		SURF		CORE	
GPS :	76.7009S, 159.304E		76.7101S, 159.343E		76.7024S, 159.3110E		76.7009S, 159.304E	
Minerals and glasses	PN [a]	Relative %	PN	Relative%	PN	Relative %	PN	Relative %
SiO_2 [b]	2	0.9	10	N.A.	-	-	-	-
Plagioclase	22	8.6	1	9.5	36	17.8	23	11.9
Alkali feldspars	5	1.1	20	5.5	1	0.07	2	0.31
Olivine	3	1.9	-	-	14	6.5	16	7.8
Clinopyroxene	9	14.8	-	-	15	10.6	29	19.2
Ca-Al-rich amphiboles [c]	52	32.2	-	-	49	16.2	21	26.6
Ca amphiboles [c]	1	0.22	-	-	-	-	3	0.7
Silicate glass	4	0.9	92	84.2	1	0.13	1	0.15
Titanomagnetite	11	1.6	1	N.A.	30	20.1	19	4.2
Ilmenite [d]	3	0.12	-	-	-	-	4	0.7
Rhönite	3	0.30	2	N.A.	1	1.1	4	0.4
Apatite	6	1.4	1	N.A.	-	-	-	-
Dolomite [e]	2	N.A.	1	N.A.	4	N.A.	1	N.A.
Unclassified	118	36.0	2	0.8	120	27.6	70	28.0
All	238	100	130	100	267	100	192	100

GPS – GPS coordinates. [a] PN = Number of particles investigated by BSE-EDS mapping. Relative% = Relative percentage by area (normalized to 100%) calculated based on the EDS analysis using the "Feature" program. N.A.—not calculated, because the particles were identified by EPMA, not by BSE-EDS . "-"—no data on the mineral or glass particles. [b] SiO_2 particle detected by BSE-EDS mapping in the BIT10 and BIT12 samples and SiO_2 inclusion analysed by fs-LA-ICP-MS in the BIT12 glassy sample. [c] Abundant metamorphic Ca-Al rich amphiboles are tschermakites (see Supplementary Dataset), whereas magmatic Ca amphiboles, such as ferrokaersutite, kaersutite and ferro-edenite were identified by EPMA in the BIT10, SURF, and CORE samples (see Table S4). [d] Ilmenite particles from samples BIT10 and CORE (major element compositions obtained by BSE-EDS) are used for temperature and f_{O2} estimations using a Fe-Ti oxide geothermobarometer as in (Ghiorso and Evans, 2008) (see Table S8). [e] Metamorphic Ca-Mg-Fe or Ca-Mg carbonates are identified among the unclassified particles (P 44, P 47, P 155, P 157 in the SURF; P 149 in the CORE; P 50 and P 22 in the BIT10, and P 84 in the BIT12, see Supplementary Dataset). A dolomite particle (analysis SURF-20, Table S9) is detected by BSE-EDS and analysed by EPMA in the SURF sample (see Table S9). Four particles of Al-rich spinel are identified (P166, 167, 168, CORE-19) in the CORE sample (see Table S8; Supplementary Dataset).

Table 2. Major and trace element compositions of "matrix" glass and "matrix" glass-hosted "inclusions" in sample BIT12 (fs-LA-ICP-MS, wt.% and ppm, respectively)

fs-LA-ICP-MS	Inclusions										Matrix (333)[$]	Model
	1	2	3	4	5	6	7	8	9	10		
wt% /ppm	G/A	G/A	G	Q	Plag An_{57}	G	G	G	G/A	G	G	Calculated melt [*] ppm
SiO_2	67.8	67.	66.	96.	52.2	73.2	64.7	66.4	67.	68.4	64.4	-
TiO_2	0.02	0.0	0.3	0.0	0.05	0.01	0.28	0.29	0.0	0.23	0.33	-
Al_2O_3	21.2	21.	17.		28.1	21.9	17.4	16.2	21.	15.2	18.2	-
MgO	0.002		0.1	-	0.056	-	0.05	0.03	-	0.04	0.16	-
MnO			0.1	-		-	0.16	0.16	-	0.13	0.18	-
FeO	0.21	0.1	5.2	-	0.34	-	5.39	5.53	0.3	4.43	5.18	-
CaO	0.46	0.8	1.2		11.42	0.31	0.96	0.79	0.2	0.75	1.20	-
Na_2O	7.2	6.5	6.7		4.8	1.5	8.0	7.6	7.7	7.8	7.6	-
Li	1.5		21	-	-		34	42	4.4	29	35	-
B	2.6	2.3	11	-	-	7.7	20	12	-	7.4	23	-
Cu			1.9	2.1	7.7	2.4	12.2	13.2		3.4	11.4	-
Zn	30	93	78		9.0	12	94	96	18	67	75	-
As			9.2	2.9		0.63	5.69	4.23		3.89	4.85	-
Rb	52.9	31.	137	-	0.68	268	200	222	75.	209	185	-
Sr	17.0	56.	7.5	-	1682	548	2.50	2.08	11.	1.40	14.7	619
Y	-		44.	-	-	-	74.6	78.9	-	65.4	66.4	-
Zr	-	0.8	585	-	-	-	100	107	-	908	835	-
Nb	-		125	-	-	-	179	208	-	197	155	-
Cs	0.15	0.0	3.3	-	0.22	2.58	5.42	6.19	-	5.56	4.52	-
Ba	104	794	28.	-	889	899	7.98	7.35	39.	4.47	108	-
La	1.43	2.7	82.	-	3.39	1.34	125	136	0.6	120	108	-
Ce	1.50	2.1	162	-	5.95	0.71	238	264	0.7	248	203	-
Pr	-	0.1	19.	-	0.53	-	27.9	28.0	-	26.1	21.7	-
Nd	-	-	63.	-	-	-	96.1	99.3	-	83.3	81.9	-
Sm	-	-	12.	-	-	-	17.4	20.0	-	13.8	14.8	-
Eu	0.39	2.6	0.8	-	2.94	3.35	0.28	0.63	0.8	0.31	1.07	-
Gd	-	-	9.9	-	-	-	13.5	16.0	-	13.5	13.4	-
Tb	-	-	1.6	-	-	-	2.54	2.12	-	2.14	2.08	-
Dy	-	-	10.	-	-	-	13.0	14.9	-	10.9	12.5	-
Ho	-	-	1.6	-	-	-	2.80	3.23	-	2.26	2.41	-
Er	-	-	3.3	-	-	-	8.94	9.53	-	5.79	7.15	-
Tm	-	-	0.8	-	-	-	0.95	1.09	-	0.73	0.95	-
Yb	-	-	5.9	-	-	-	6.37	8.91	-	6.28	6.39	-
Lu	-	-	1.2	-	-	-	1.22	0.75	-	0.67	0.98	-
Hf	-	-	14.	-	-	-	24.0	24.8	-	18.9	18.5	-
Ta	-	-	6.9	-	-	0.31	11.2	12.6	-	9.71	9.26	-
Pb	1.86	2.4	14.	-	-	113	22.7	26.8	2.1	17.7	18.5	-
Th	-	-	18.	-	-	-	29.4	31.0	-	20.7	23.6	-
U	-	-	4.3	-	-	-	7.51	8.61	-	5.76	5.77	-

G = glass; Q = quartz; Plag = plagioclase; A = anorthoclase; * Melt composition is calculated based on the partition coefficients between plagioclase and melt according to (Bindeman et al., 1998) and

847 analysis № 5 for the plagioclase. Blanks in the columns represent values below the detection limits
848 of fs-LA-ICP-MS. 1–10 are the compositions of minerals and glass “inclusions” in the glassy matrix
849 (“matrix”). $ Bracketed number indicates number of points per analysis.

850